

# *A Risk-Aware Path Planning Strategy for UAVs in Urban Environments*

**Stefano Primatesta, Giorgio Guglieri & Alessandro Rizzo**

**Journal of Intelligent & Robotic Systems**  
with a special section on Unmanned Systems

ISSN 0921-0296  
Volume 95  
Number 2

J Intell Robot Syst (2019) 95:629-643  
DOI 10.1007/s10846-018-0924-3



**Your article is protected by copyright and all rights are held exclusively by Springer Nature B.V.. This e-offprint is for personal use only and shall not be self-archived in electronic repositories. If you wish to self-archive your article, please use the accepted manuscript version for posting on your own website. You may further deposit the accepted manuscript version in any repository, provided it is only made publicly available 12 months after official publication or later and provided acknowledgement is given to the original source of publication and a link is inserted to the published article on Springer's website. The link must be accompanied by the following text: "The final publication is available at [link.springer.com](http://link.springer.com)".**



# A Risk-Aware Path Planning Strategy for UAVs in Urban Environments

Stefano Primatesta<sup>1</sup> · Giorgio Guglieri<sup>2</sup> · Alessandro Rizzo<sup>3</sup>

Received: 15 May 2018 / Accepted: 17 August 2018 / Published online: 6 September 2018  
© Springer Nature B.V. 2018

## Abstract

This paper presents a risk-aware path planning strategy for Unmanned Aerial Vehicles in urban environments. The aim is to compute an effective path that minimizes the risk to the population, thus enforcing safety of flight operations over inhabited areas. To quantify the risk, the proposed approach uses a risk-map that associates discretized locations of the space with a suitable risk-cost. Path planning is performed in two phases: first, a tentative path is computed off-line on the basis on the information related to static risk factors; then, using a dynamic risk-map, an on-line path planning adjusts and adapts the off-line path to dynamically arising conditions. Off-line path planning is performed using riskA\*, an ad-hoc variant of the A\* algorithm, which aims at minimizing the risk. While off-line path planning has no stringent time constraints for its execution, this is not the case for the on-line phase, where a fast response constitutes a critical design parameter. We propose a novel algorithm called *Borderland*, which uses the *check and repair* approach to rapidly identify and adjust only the portion of path involved by the inception of relevant dynamical changes in the risk factor. After the path planning, a smoothing process is performed using Dubins curves. Simulation results confirm the suitability of the proposed approach.

**Keywords** Path planning · Unmanned aerial vehicles · Risk-map · Risk-aware path planning · RiskA\* · Borderland algorithm

## 1 Introduction

Unmanned Aerial Vehicles (UAVs) are gaining momentum in recent years and their extensive use has induced the rapid growth of related research areas. UAVs have been successfully used in several applications, both in military and in civil fields, such as security surveillance, search and rescue, environmental monitoring, and mapping, to name a few [2]. In particular, the use of UAVs in urban environments is steadily growing and, in the very near future, UAVs will be involved in Smart Cities [18, 31]. For

this reason, it will be mandatory to enhance safety of flight operations.

Path planning is one of the key elements to provide autonomy to UAVs in the execution of missions, by defining the set of waypoints to reach a destination, while satisfying some optimality criterion [11]. Path planning has been widely studied and a large number of methods have been proposed in the last decades. Starting in the late 50s with the Dijkstra algorithm [7], graph search algorithms have been widely used in path planning. One of the most commonly used algorithms is A\* [15], which complements the logic of graph search with a heuristic component for the computation of the cost function. Several A\*-based algorithms have been developed for dynamic [40] and anytime [27] path planning, and in high dimensional environments [16, 17].

Another popular family of path planning algorithms comprises sample-based techniques, which explore the search space through a sampling scheme. Widely diffused approaches are Probabilistic Roadmaps (PRM) [22] and Rapidly-exploring Random Trees (RRT) [25]. Especially RRT is very popular, and many RRT-based algorithms have been developed. The most popular is RRT\* [20], a near-optimal version of RRT, also used to perform kinodynamic

---

✉ Alessandro Rizzo  
alessandro.rizzo@polito.it

<sup>1</sup> Department of Control and Computer Engineering, Politecnico di Torino, Corso Duca degli Abruzzi 24, 10129 Turin, Italy

<sup>2</sup> Department of Mechanical and Aerospace Engineering, Politecnico di Torino, Corso Duca degli Abruzzi 24, 10129 Turin, Italy

<sup>3</sup> Department of Electronics and Telecommunications, Politecnico di Torino, Corso Duca degli Abruzzi 24, 10129 Turin, Italy

path planning [21]. Sample-based algorithms have been also used for UAVs [44].

A wide variety of path planning algorithms specifically dedicated to UAVs has been presented in the literature. In [29] the authors propose a kinodynamic path planning algorithm with collision avoidance using the Closed-loop RRT. Other techniques are based on evolutionary algorithms (EAs) [36], as well as reinforcement learning approaches [46]. Often, path planning for UAVs uses techniques based on an explicit 3D description of the environment [6, 45].

When autonomous vehicles move in uncertain or populated environments, risk should be accounted for to produce an effective and safe path planning. In [43] the authors propose a dynamic path planning for UAVs that takes into account static and dynamic threats. In [5, 42] risk-maps are used to compute the path with minimum risk. Risk-aware path planning is a common problem in robotics and concerns also mobile robots [10] and autonomous underwater vehicles (AUVs) [33]. In general, risk-aware path planning takes into account risk factors emerging from the UAV point of view, i.e., it minimizes the risk of collision with obstacles and other vehicles [38, 43]. However, when UAVs operate in urban environments, it should be mandatory to consider the risk to people on the ground. In [39] the authors propose a path planning algorithm for emergency landing, in order to avoid populated areas. Another work introduces a path planning technique minimizing the trade off between risk to the population and flight time [37]. In [12], Guglieri et al. propose a path planning strategy for UAVs using the RA\* algorithm, a modified version of A\* that takes into account the risk of flying over a given area.

The risk to the population is defined by risk analysis. A common risk assessment approach defines the risk as the probability of lethal incidents when the UAV flies over a populated area [3, 4, 13, 24].

## 1.1 Current Work

This work introduces a new perspective in path planning, whereby the definition of optimal path accounts for both static and dynamic risk factors for the population on ground along the route. The proposed path planning algorithm takes a so-called risk-map in input. A risk-map is a dynamical location-based map, where each location is associated with a specific risk-cost that quantifies the risk of flying over that location [4, 13]. The proposed path planning approach is composed by an off-line and an on-line path planning phase.

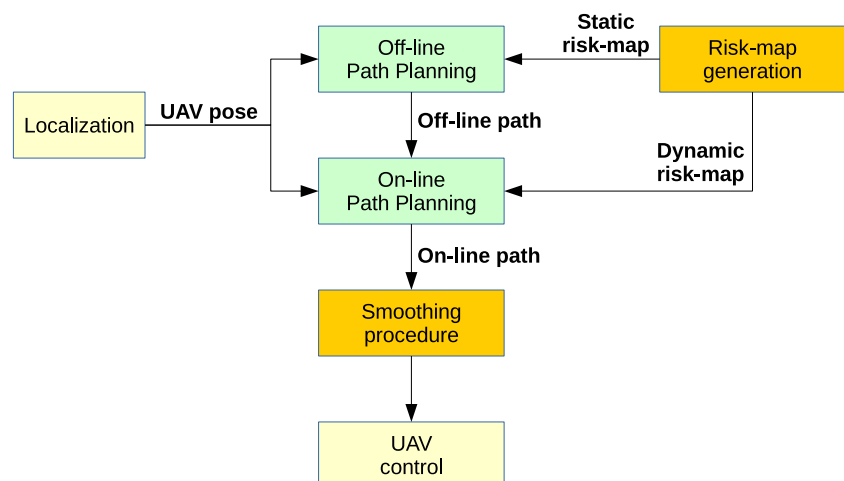
First, the off-line path planning aims to solve an optimal path planning problem. Given a risk-map, a starting and a final point, the off-line path planning seeks for a globally optimal path that avoids obstacles and no-flight areas, computed minimizing the risk-cost defined by the risk-map. The off-line path is computed before the mission starts and, in general, when the UAV is still on the ground. Thus, the off-line path planning is not, in general, a time-critical activity.

The on-line path planning aims to repair and adapt the off-line path in real-time, according to relevant information emerging from a dynamic risk-map. During the trajectory execution, in fact, the risk-map changes when unanticipated obstacles and other risk factors appear. For this reason the on-line path planning only focuses on the portion of path not already executed, i.e., from the current position of the UAV to the target point. Unlike off-line planning, the on-line one is time-critical, since the UAV is already flying en-route and needs to react promptly to dynamically changing conditions.

After path planning, a fast path smoothing procedure based on Dubins curves [8] is applied to the obtained path. This procedure is needed in order to transform the theoretically-obtained path in a flyable one. Then, the path is handed over to a UAV Control System [41]. Figure 1 illustrates the architecture of the proposed approach.

Guidelines for the development of our approach have been introduced for the first time in [34], as a part

**Fig. 1** The main architecture of the proposed risk-aware path planning approach



of a Cloud-based framework for risk-aware intelligent navigation for UAVs in urban environments.

This paper is organized as follows. Section 2 provides an overview on risk assessment and risk-maps. Then, in Section 3, the off-line path planning is illustrated in detail, focusing on the problem formulation and on riskA\*, our proposed algorithm. Section 4 describes the on-line path planning, achieved through the novel Borderland algorithm. Then, in Section 5 the path smoothing procedure using Dubins curves is described. Finally, in Section 6 the proposed method is validated by numerical results. Our conclusions are drawn in Section 7.

## 2 Risk-map

This section provides an overview of basic concepts about the definition of the risk-map.

In path planning problems, the construction of a map has a critical role, since it defines the search space, i.e., the space with all the possible configurations where the path planning algorithm searches for the solution [26]. The risk-map used in this work is a dynamic one that quantifies the risk of flying over a given position, including the presence of obstacles. The risk-map describes a discretized 2D space, i.e., flight at constant and fixed altitude is considered. A location-based map is assumed, where the 2D space is sampled in a grid fashion and each location is associated with a number, quantifying the risk level [13]. Thus, a map  $M$  consists of a  $n \times m$  matrix of locations:

$$M = \begin{Bmatrix} r_c(p_{1,1}) & r_c(p_{1,2}) & \cdots & r_c(p_{1,m}) \\ r_c(p_{2,1}) & r_c(p_{2,2}) & \cdots & r_c(p_{2,m}) \\ \vdots & \vdots & \ddots & \vdots \\ r_c(p_{n,1}) & r_c(p_{n,2}) & \cdots & r_c(p_{n,m}) \end{Bmatrix}, \quad (1)$$

where each element  $r_c(p_{i,j})$  refers to a square cell centered in the location  $p_{i,j}$  and with a specific dimension. The dimension of the cell, i.e. the risk-map resolution, is defined considering the quality of the source data used to generate the risk-map. Each element  $r_c(p_{i,j})$  is the risk-cost associated to the referred cell, and is expressed by a real number in the range [0,1]. Notably, 0 corresponds to a zone with no risk, while 1 defines a zone with the highest flight risk, i.e. a no-flight zone.

The risk-cost value is defined according to [3, 4, 13, 24]. In particular, the risk-cost is proportional to the hourly probability of lethal incidents, defined as the succession of three conditional events: (i) the loss of control of the vehicle with uncontrolled crash on the ground, (ii) the impact with someone, and (iii) a fatal injury to the person that has been hit. This hourly probability is therefore defined as follows:

$$P_{casualty}(p_{i,j}) = P_{crashing} \times P_{impact}(p_{i,j}) \times P_{fatality}(p_{i,j}). \quad (2)$$

The probability of crashing  $P_{crashing}$  is the probability of loss of control of the UAV with the uncontrolled crash on the ground. This term is expressed as a rate per hour ( $h^{-1}$ ) and it generally coincides with the failure rate of the aircraft. Its value depends on the vehicle type and its reliability. In [4], a constant value in the range  $[10^{-6}, 10^{-9}] h^{-1}$  is used for generic unmanned aircraft systems, while in [23] values in the range  $[0.5, 10] h^{-1}$  are established for Micro Air Vehicles (MAVs).

The probability of impact with someone  $P_{impact}(p_{i,j})$  considers the crashing area  $A_{crash}$  and the population density  $\rho$  relative to the position  $p_{i,j}$ :

$$P_{impact}(p_{i,j}) = \rho(p_{i,j}) \cdot A_{crash}. \quad (3)$$

The crashing area is computed according to the method used in [4], taking into account the dimensions of the UAV and of the average human being.

The probability of fatal injury  $P_{fatality}(p_{i,j})$  is defined using the approach proposed in [4], accounting for the sheltering factor relative to the position  $p_{i,j}$  and the kinetic energy at impact. The sheltering factor defines how the population is exposed to the impact of the UAV. In fact, the presence of obstacles in the impact area can reduce the probability of fatal injuries, because obstacles can absorb the impact energy and provide shelter to debris.

In order to ensure an appropriate level of safety, a maximum value of  $P_{casualty}$  is specified. According to the "Equivalent Level of Safety" defined in [4, 13], an appropriate and conservative value of *maximum acceptable risk* is  $10^{-6} h^{-1}$ . The risk-cost value is computed for each location  $p_{i,j}$  in the risk-map, then it is normalized in the range [0,1], whereas 1 defines locations with a risk-cost value greater than the maximum acceptable risk. Obstacles at the flight altitude and no-fly zones enforced by National aviation agencies are accounted for by forcing the corresponding risk-cost to 1.

## 3 Off-line Path Planning

The off-line path planning takes as input the risk-map and solves a risk-aware path planning problem before the beginning of the flight mission. Since the risk-map is defined at fixed flight altitude, a two-dimensional path planning problem is here tackled.

Here, off-line path planning is realized through an A\*-based [15] graph search algorithm, called riskA\*, which optimizes the path by trading off risk-cost and path length.

### 3.1 Problem Formulation

Let  $C \subseteq \mathbb{R}^2$  be a continuous search space of a path planning problem. As in many other applications [32],  $C$  is

discretized into a discrete space  $X$ , on which the risk-map will be constructed, and taking into account the risk-map resolution. Each state  $x \in X$  is a discrete location in the discrete search space. With a slight abuse of notation, here and henceforth we will refer to  $x$  as a state of search space, a location of the risk-map  $M$ , or a node of a search grid graph.

The obstacle region  $X_{obs} \subseteq X$  is the set of locations in which flight is forbidden. Thus, the associated cost is equal to 1, as described in Section 2. The set  $X_{free} = X \setminus X_{obs}$  contains the remaining navigable locations. The initial and final locations are denoted  $x_{start}, x_{goal} \in X_{free}$ . Let  $\Sigma$  be the set of all paths, where a single path  $\sigma$  is a sequence of connected locations  $x$  in the search space  $X$ . The path planning algorithm searches for an optimal path  $\sigma^*$  from  $x_{start}$  to  $x_{goal}$  in  $X_{free}$ , which minimizes a given cost function  $f : \Sigma \rightarrow \mathbb{R} \geq 0$ . Hence, the optimal path is the solution of the following program:

$$\begin{aligned} \sigma^* &= \arg \min_{\sigma \in \Sigma} f(\sigma(s)) \\ \text{subject to } \sigma(0) &= x_{start} \\ \sigma(1) &= x_{goal} \\ \forall s \in [0, 1], \sigma(s) &\in X_{free}. \end{aligned} \tag{4}$$

### 3.2 RiskA\* Algorithm

The riskA\* algorithm is based on the well-known A\* [15]. Similarly to the A\* algorithm, the input of riskA\* is a graph  $M$  composed by nodes and edges. Here, we specialize the algorithm by considering a two-dimensional grid graph, where each location corresponds to a graph node, and each portion of path between two nodes corresponds to a graph edge. The output of riskA\* is a back-pointer path, which is a sequence of nodes, starting from the goal and tracing back to the start.

Similarly to A\*, the general idea of riskA\* is to move through the graph minimizing the cost function

$$f(x) = g(x) + k \cdot h(x), \tag{5}$$

where  $g(x)$  is the motion cost of the path from node  $x$  to the start node  $x_{start}$ , the constant  $k$  is the adjustment variable, and  $h(x)$  the heuristic cost, i.e., the estimated motion cost of the best path between  $x$  and  $x_{goal}$ . Thus,  $f(x)$  is the estimated motion cost corresponding to the shortest path from  $x_{start}$  to  $x_{goal}$ , passing through node  $x$ .

Differently from traditional A\*, riskA\* encapsulates the risk-cost in the cost function  $f(x)$ . Given a generic node  $x_n$ , the motion cost  $g(x_n)$  is

$$g(x_n) = \int_{x_{start}}^{x_n} r_c(x) dx, \tag{6}$$

where  $g(x_n)$  is the integral of the risk-cost between the initial state  $x_{start}$  and state  $x_n$ . Function  $r_c(x)$  is the risk-cost

associated with the path. Similarly, the heuristic function cost  $h(x_n)$  is

$$h(x_n) = \int_{x_n}^{x_{goal}} r_c(x) dx, \tag{7}$$

where  $h(x_n)$  is the integral of the risk-cost between state  $x_n$  and the final state  $x_{goal}$ .

The risk-cost function takes values in  $0 < r_c(x) \leq 1$ . As a consequence, the motion cost is never equal to zero. Moreover, conservative considerations lead us to never consider the risk equal to zero.

Figure 2a exemplifies the cost function  $f(x)$  at step  $n$ . Note that  $g(x)$  is the effective motion cost from the initial node, while  $h(x)$  is the estimated motion cost until the final node. Hence,  $g(x)$  and  $h(x)$  are complementary along the path.

The riskA\* algorithm is described in Algorithm 1. Its inputs are  $x_{start}$  and  $x_{goal}$ , and a grid graph  $M$  related to the risk-map. Similarly to A\*, two data structures are used, called  $O$  (Open set) and  $C$  (Closed set). The Open set is used to store currently discovered nodes waiting to be

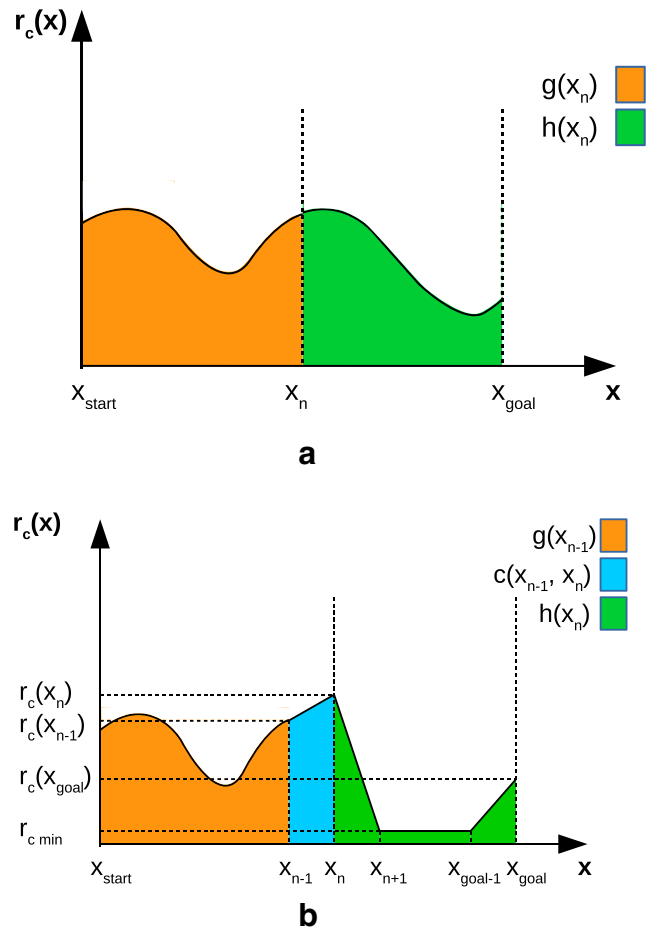


**Fig. 2** Graphical exemplification of the cost function  $f(x)$ . Given a generic state  $x_n$ , in **a** the cost function is composed by the motion cost  $g(x_n)$  and the heuristic cost  $h(x_n)$ . In **b**, the incremental step defined in Eqs. 8, 9, 10, and 11 is illustrated

evaluated. Set  $O$  is a priority queue defined according to the estimated cost  $f(x)$ , such that an element with low cost is served before an element with high cost. The Closed set is the set of nodes already processed or invalid. The algorithm uses the same logic of A\*. Important variants with respect to the original algorithm are in lines 6, 7, where if more than one node  $x_{best}$  with the same motion cost exist, the algorithm selects the node with the lower risk-cost. The riskA\* algorithm generates a search tree, which, by definition, has no cycles.

**Algorithm 1** riskA\* algorithm

```

1: procedure RISKASTARSEARCH( $x_{start}, x_{goal}, M$ )
2:   Add  $x_{start}$  to  $O$ 
3:   Add all invalid nodes  $x_{invalid} \in M$  to  $C$ 
4:   repeat
5:     Pick  $x_{best}$  from  $O$  with  $f(x_{best}) \leq f(x), \forall x \in O$ 
6:     if  $\exists$  multiple  $x_{best}$  then
7:       Pick the  $x_{best}$  with lower  $r_c(x_{best})$ 
8:     end if
9:     Remove  $x_{best}$  from  $O$  and add to  $C$ 
10:    if  $x_{best} = x_{goal}$  then
11:      return ReconstructPath( $x_{goal}, x_{start}$ )
12:    end if
13:    Expand  $x_{best}$ : for all  $x_{adj} \in \text{Near}(x_{best})$  and
       $x_{adj} \notin C$ 
14:    if  $x_{adj} \notin O$  then
15:      Add  $x_{adj}$  to  $O$ 
16:      else if  $g(x_{best}) + c(x_{best}, x_{adj}) < g(x_{adj})$  then
17:        Update  $x_{adj}$ 's backpointer to point to  $x_{best}$ 
18:      end if
19:    until  $O$  is empty
20:    return ReconstructPath( $x_{goal}, x_{start}$ )
21: end procedure

```

For each node  $x$  explored by riskA\*, the estimated cost function  $f(x)$  is computed as described in Eqs. 5, 6, and 7. Considering the discrete grid, the integral is computed with an approximate and incremental method. Thus,  $g(x_n)$  is the sum of the motion cost at the previous step  $g(x_{n-1})$  and the trapezoidal area described by the motion cost from  $x_{n-1}$  and  $x_n$ , denoted with  $c(x_{n-1}, x_n)$ :

$$\begin{aligned}
 g(x_n) &= \int_{x_{start}}^{x_{n-1}} r_c(x)dx + \int_{x_{n-1}}^{x_n} r_c(x)dx \\
 &= g(x_{n-1}) + c(x_{n-1}, x_n),
 \end{aligned}
 \tag{8}$$

with

$$c(x_{n-1}, x_n) = \frac{r_c(x_{n-1}) + r_c(x_n)}{2} \text{dist}(x_{n-1}, x_n),
 \tag{9}$$

where  $\text{dist}(x_{n-1}, x_n)$  is the Euclidean distance between two nodes. Figure 2b illustrates the discretization of the cost function.

The term  $h(x_n)$  quantifies the area described by the estimated motion cost from  $x_n$  and the final state  $x_{goal}$ . With A\*-based algorithms, if an admissible heuristic is adopted, the algorithm is able to search for the optimal solution in the graph. The heuristic  $h(x_n)$  is admissible if  $h(x_n) \leq h^*(x_n)$  for each node  $x_n$ , and with  $h^*(x_n)$  being the effective optimal motion cost from  $x_n$  to the goal. If the heuristic is not admissible, the A\*-based algorithm may overestimate the motion cost to reach the goal, and it may overlook nodes that would lead to the optimal solution. Then, in order to have an admissible heuristic, we estimate the motion cost considering the minimum risk-cost between nodes  $x_n$  and  $x_{goal}$ . Then, as depicted in Fig. 2b, the heuristic cost is computed as follows:

$$\begin{aligned}
 h(x_n) &= \frac{r_c(x_n) + r_{c \min}}{2} \text{dist}(x_n, x_{n+1}) + \text{dist}(x_{n+1}, x_{goal-1})r_{c \min} + \\
 &\quad + \frac{r_c(x_{goal}) + r_{c \min}}{2} \text{dist}(x_{goal-1}, x_{goal}),
 \end{aligned}
 \tag{10}$$

where  $r_{c \min} > 0$  is the minimum value of the risk-cost function. Assuming

$$\text{dist}(x_n, x_{n+1}) = \text{dist}(x_{goal-1}, x_{goal}) = \text{dist}_{\min},$$

with  $\text{dist}_{\min}$  the minimum distance between two adjacent nodes, the heuristic function becomes:

$$\begin{aligned}
 h(x_n) &= \frac{r_c(x_n) + r_c(x_{goal})}{2} \text{dist}_{\min} + \\
 &\quad + (\text{dist}(x_n, x_{goal}) - \text{dist}_{\min})r_{c \min}.
 \end{aligned}
 \tag{11}$$

A\*-based algorithms are able to find the optimal solution in the graph. However, due to the discrete space, the outcome of A\*-based algorithms may not be the optimal one in the continuous space. In fact, the path computed with riskA\* is constrained to express turn angles that are multiple of 45°. A post-optimization phase is therefore performed after the execution of riskA\*.

Post-optimization is described in Algorithm 2. The algorithm explores the path (lines 3 to 12). Then, considering two states  $x_j, x_k \in \sigma$ , the algorithm verifies if the line of sight segment  $\text{LOS}(x_j, x_k)$  improves the path. The  $\text{LOS}(\cdot)$  segment connects two nodes  $x_j$  and  $x_k$  with a straight line in the continuous space, inserting additional nodes using a linear interpolation (line 4). The interpolation step is comparable with the risk-map resolution. Then, the motion cost  $\text{cost}(\cdot)$  of the  $\text{LOS}(\cdot)$  segment is computed using the incremental method described in Eqs. 8 and 9. If the  $\text{LOS}(x_j, x_k)$  segment has a lower motion cost than the path from  $x_j$  to  $x_k$ , referred as segment  $(x_j, x_k)$ , the algorithm updates the path (line 6). Moreover, after the replacement of the  $\text{LOS}(\cdot)$  segment, the  $k$  index needs to be updated accounting for the updated path (line 7). This iterative procedure continues until the  $x_{goal}$  node is reached. A simple example of the post-optimization procedure is illustrated in Fig. 3.

We remark that the post-optimization procedure aims to optimize the path locally, since the global optimization is provided by the riskA\* algorithm.

**Algorithm 2** Post-optimization algorithm

```

1: procedure POSTOPTIMIZATION( $\sigma$ )
2:    $j = 1, k = 3$ 
3:   while  $j \neq \text{length}(\sigma)$  do
4:     Interpolate(LOS( $x_j, x_k$ ))
5:     if  $\text{cost}(\text{LOS}(x_j, x_k)) \leq \text{cost}(\text{segment}(x_j, x_k))$ 
6:       then
7:         Replace  $\text{segment}(x_j, x_k) \in \sigma$  with
8:           LOS( $x_j, x_k$ )
9:         Update  $k$ 
10:         $k = k + 1$ 
11:       else
12:         $j = j + 1$ 
13:       end if
14:     end while
15:   return  $\sigma$ 
16: end procedure
    
```

**4 On-line Path Planning**

**4.1 Problem Formulation**

The on-line path planning is based on a *check and repair* approach [9], in which the path is dynamically adapted in accordance to a dynamic risk-map.

Recalling the notation of the off-line path planning problem described in Section 3.1, the off-line path  $\sigma$  is a sequence of locations  $x \in X_{\text{free}}$  from  $x_{\text{start}}$  to  $x_{\text{goal}}$ . Considering the dynamic risk-map, the search space  $X(k)$  changes at each discrete-time step  $k$ , then the path is considered as a sequence of states  $x(k)$ .

Hence, at each time step, the differential search space  $X_{\text{diff}}(k)$  can be defined as follows:

$$X_{\text{diff}}(k) = X(k) - X(k - 1). \tag{12}$$

Moreover, the on-line path planning algorithm aims to repair the path only when it is necessary, i.e., when the path involves an area with increased risk-costs. For this reason, a differential risk-map  $M_{\text{diff}}$  related to  $X_{\text{diff}}$  is defined as

$$M_{\text{diff}}(x_n(k)) = \begin{cases} 1 & \text{if } \Delta r_c(x_n(k)) > 0, \\ 0 & \text{otherwise,} \end{cases} \tag{13}$$

with

$$\Delta r_c(x_n(k)) = r_c(x_n(k)) - r_c(x_n(k - 1)). \tag{14}$$

The differential risk-map  $M_{\text{diff}}$  has the same dimension of the risk-map  $M$ . The notation  $M_{\text{diff}}(x_n(k))$  defines the state of the generic node  $x_n$  in the differential map  $M_{\text{diff}}$  at time  $k$ . Figure 4 illustrates an example of risk-maps at time  $k$  and  $k - 1$ , and the corresponding differential map.

The *check* routine verifies if  $M_{\text{diff}}(x(k)) > 0, \forall x(k) \in \sigma$ , i.e., it verifies which part of the path has to be updated due to a change in the risk-map.

The *Repair* routine tries to adjust the path with a fast algorithm, in order to tackle the dynamic risk-map.

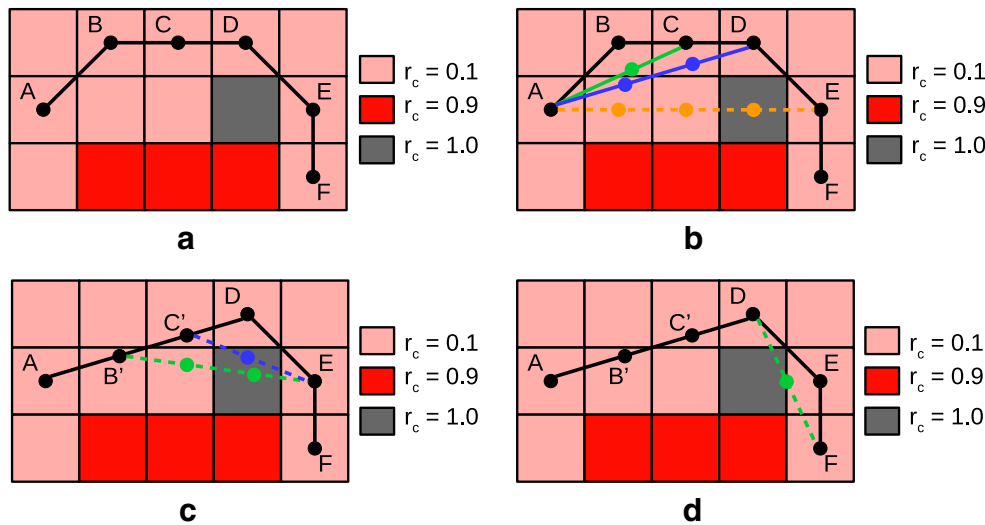


**Fig. 3** Simple example of the post-optimization procedure. In **a**, the path is computed with riskA\*, as a sequence of nodes from A to F. In **b**, the post-optimization procedure searches for LOS(·) segments that improve the path. Starting from node A, it considers at first the LOS(A, C), then the LOS(A, D). On the contrary, it discards the

LOS(A, E), because it crosses a high risk area. In **c**, the path is updated with the segment A-B'-C'-D, with B' and C' being the interpolated nodes of the LOS(A, D). Then, the post-optimization procedure discards the LOS(B', E) and the LOS(C', E), as well as the LOS(D, F) in **d**

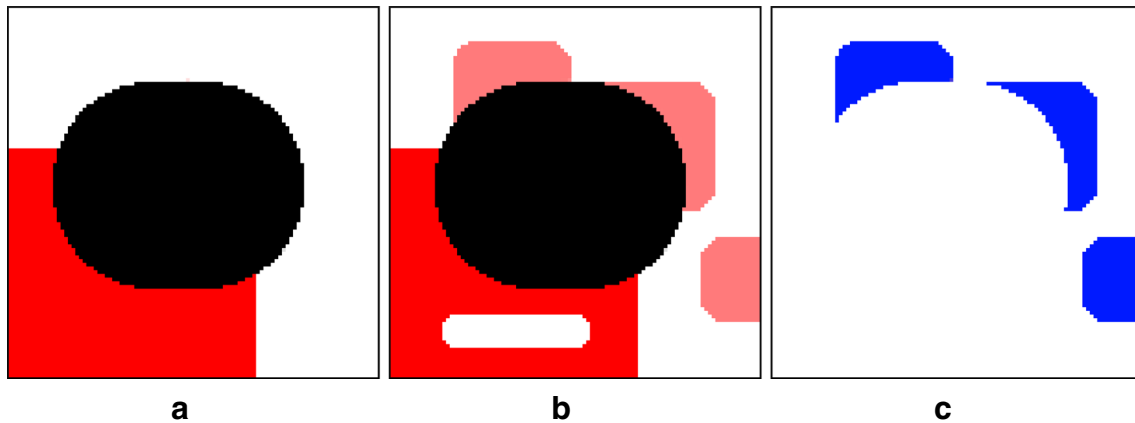


**Fig. 4** Example of the differential risk-map construction, in which the risk areas are identified: white areas have minimum risk-cost, black areas have maximum risk-cost, and shade of red areas have middle

cost, with darker red areas associated with higher risk-cost. In **a**, the risk-map at time  $k - 1$ . In **b**, the risk-map at time  $k$ . In **c**, the differential risk-map defined according to Eq. 13

RiskA\* is not suitable to solve this problem, because of its high computational time, since it requires a time proportional to the dimension of the map. Unlike off-line path planning, the on-line algorithm needs to adapt the path in a short time, because the UAV is currently executing the mission. As a consequence, the on-line path planning needs to trade off between computational burden and optimality.

In the following, we propose the Borderland algorithm as a solution to the on-line path planning problem.

### 4.2 Borderland Algorithm

Borderland algorithm is an extension of Bug algorithms [30] applied to grid graphs and with generic motion cost. Bug-based algorithms are widely used in on-line path planning to tackle complex and dynamic environments [1, 19]. In our approach, the idea is to follow the contour of each risk area involved and circumnavigate it, in order to adjust the path minimizing the combination of risk-cost and path length.

The pseudo code of the Borderland algorithm is described in Algorithm 3. The inputs are: (i) the current UAV position at time  $k$ , (ii) the most recent path computed at time  $k - 1$ , (iii) the grid graph search space  $M$  at time  $k$ , related to  $X$ , and (iv) the differential space  $M_{diff}$  related to  $X_{diff}$ . The Borderland algorithm always considers the path from the current UAV position to the goal, because the previous portion of the path is already executed.

First, the algorithm visits each location  $x$  in the path  $\sigma$  and checks if each  $x$  is involved in the differential risk-map. If this is the case, it adds  $x$  to a differential set  $D$  (lines 2 to 5). The differential set  $D$  is a set of nodes belonging to the path  $\sigma$  and contained in the differential risk-map  $M_{diff}$ .

From all locations in  $D$ , Borderland detects path segments  $S[x_a, x_b]$  as sequences of locations (line 7). Segments  $S[x_a, x_b]$  are the portions of path that need to be repaired.

---

#### Algorithm 3 Borderland algorithm

---

```

1: procedure BORDERLANDSEARCH( $x_{pos}, \sigma, M, M_{diff}$ )
2:   for each  $x \in \sigma$  do
3:     if  $M_{diff}(x) > 0$  then
4:       Add  $x$  to  $D$ 
5:     end if
6:   end for
7:   Detect segments  $S[x_a, x_b]$  as a sequence of  $x \in D$ 
8:   for each  $S[x_a, x_b]$  do
9:     if  $x_a \in S[x_a, x_b] = x_{pos}$  then
10:      Search nearest  $x_{esc}$  with  $M_{diff}(x_{esc}) = 0$ 
11:      Search for  $\sigma_{seg}[x_a, x_b]$  through  $x_{esc}$ 
12:     else
13:        $\sigma_{seg} = \text{Circumnavigate area}(M_{diff} > 0)$ 
14:       if  $\nexists \sigma_{seg}$  then
15:         if  $r_c(\text{area}(M_{diff} > 0)) < 1$  then
16:           Reduce  $\text{area}(M_{diff} > 0)$  until  $\exists \sigma_{seg}$ 
17:         else if  $r_c(\text{area}(M_{diff} > 0)) = 1$  then
18:           Search  $\sigma_{seg}[x_a, x_b]$  in  $M$ 
19:         end if
20:       end if
21:     end if
22:     if  $\exists \sigma_{seg}$  then
23:       if  $\text{cost}(\sigma_{seg}) > \text{cost}(S[x_a, x_b])$  then
24:         Discard  $\sigma_{seg}$ 
25:       end if
26:     else
27:        $\nexists$  solution
28:     return
29:   end if
30: end for
31: Reconstruct Path  $\sigma_{new}$  with  $\sigma$  and every  $\sigma_{seg}$ 
32: Simplify  $\sigma_{new}$ 
33: return  $\sigma_{new}$ 
34: end procedure

```

---

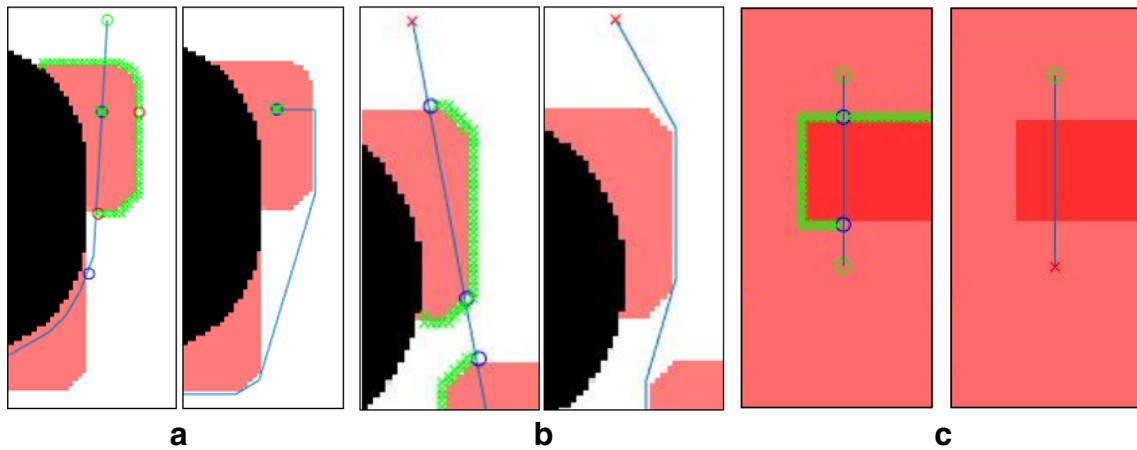


**Fig. 5** Examples of Borderland scenarios. After the update of the risk-map, in **a**, the current position is in a high risk area. Thus, an escape route is computed, finding an alternative path with lower cost. In **b**, a common scenario, where the algorithm circumnavigates the risk area

with a path with lower motion cost. In **c**, the algorithm tries to circumnavigate the risk-area. The alternative path has a greater cost than the original one, consequently, the route is not modified

Here, the algorithm checks if the current position  $x_{pos}$  is contained in the segment  $S[x_a, x_b]$ . In the affirmative case, it searches for an escape location  $x_{esc}$  outside of the differential risk-map and seeks for an alternative segment  $\sigma_{seg}$ , passing through  $x_{esc}$  (lines 9 to 11).

Hence, for each  $S[x_a, x_b]$ , the Borderland algorithm tries to circumnavigate the differential area in  $M_{diff}$  with a new portion of path  $\sigma_{seg}$  (line 13) as an alternative segment.

If such an  $\sigma_{seg}$  segment does not exist and the involved area in  $M_{diff}$  has a risk-cost strictly lower than 1 (i.e. it is not an obstacle or a no-flight area), the algorithm searches for an alternative path, by reducing the involved area  $M_{diff}$  until a segment  $\sigma_{seg}$  exists (lines 15, 16). This means that the algorithm searches for an alternative path in the differential map (see Fig. 6).

Otherwise, if the involved area is a no-fly zone, it is impossible to find a local solution in the differential risk-map. Thus, the algorithm seeks for a solution in the risk-map  $M$ , circumnavigating no-fly zones (lines 17, 18).

If a feasible portion of path  $\sigma_{seg}$  exists, the Borderland algorithm compares the motion cost of the new segment  $\sigma_{new}$  with the old one  $S[x_a, x_b]$ . If the former has a greater cost, then it discards  $\sigma_{seg}$  (lines from 22 to 25).

On the contrary, if a solution does not exist, the algorithm reports this issue.

Once all segments have been examined, the new path  $\sigma_{new}$  is reconstructed using the old path  $\sigma$  and segments  $\sigma_{seg}$  (line 31). Finally, the algorithm modifies the path  $\sigma_{new}$  with the post-optimization procedure described in Algorithm 2 (line 32).

In order to clarify how the Borderland algorithm works, in Figs. 5 and 6 some simple scenarios are illustrated. In Fig. 5a, the current position is in the high risk area due to a dynamic update of the risk-map. The algorithm searches for

an escape location outside of the updated differential space and it finds an alternative path.

Figure 5b shows a typical scenario, in which the algorithm circumnavigates the high risk area and finds a path with lower cost. On the contrary, in Fig. 5c, the new route computed by Borderland has a greater cost than the previous one, therefore it is discarded.

In the scenario of Fig. 6, the Borderland algorithm searches for an alternative path. In order to find a solution, the algorithm reduces the involved area and the resulting path minimizes the motion cost.

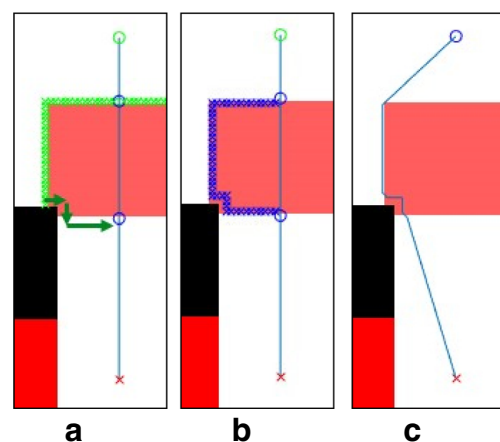


**Fig. 6** Example of Borderland scenario. After the update of the risk-map, in **a**, the path crosses the area with high risk-cost. The algorithm searches for an alternative path. As there is no solution, the algorithm searches for the solution in the differential map by *reducing* the involved area, until an alternative path is found (**b**). In **c** the final solution is illustrated

### 5 Path Smoothing Using Dubins Curves

After the path planning procedure, the theoretical path is still not suitable for UAVs. Even if the post-optimization procedure solves the path constraints to grid edges, the resulting path may not be performed by aerial vehicles because of kinematic constraints. In order to achieve a more suitable and realistic path, a smoothing procedure is required. Due to their simplicity and performance, Dubins curves constitute a viable solution.

Dubins curves are introduced in [8] and refer to the shortest curve between two poses in the two-dimensional plane considering constraints in the radius of curvature. Assuming a constant speed of the vehicle and the state of the UAV,  $q = (q_x, q_y, q_\theta)$ , the differential equation describing Dubins curves are:

$$\dot{q}_x = \cos(q_\theta) \tag{15}$$

$$\dot{q}_y = \sin(q_\theta) \tag{16}$$

$$\dot{q}_\theta = u, \tag{17}$$

with  $u$  normalized between  $-1$  and  $1$  with respect to the maximum curvature radius. According to [8], the shortest path between two poses is always expressed as a combination of no more than three motion primitives. For this reason, only three values of  $u$  are used, that is  $u \in \{-1, 0, 1\}$ . For simplicity, the value  $0$  describes a straight motion (S), while  $-1$  and  $1$  are the right (R) and left (L) turn, respectively. As a consequence, only six combinations of curves are admissible:

$$\{LRL, RLR, LSL, LSR, RSL, RSR\}. \tag{18}$$

In Fig. 7, the path smoothing procedure using Dubins curves is illustrated.

Often, smoothing using Dubins curves is performed during the path planning phase, whereby the path is defined considering the curvature radius of the vehicle [14, 28]. Sometimes, this approach is preferable because the

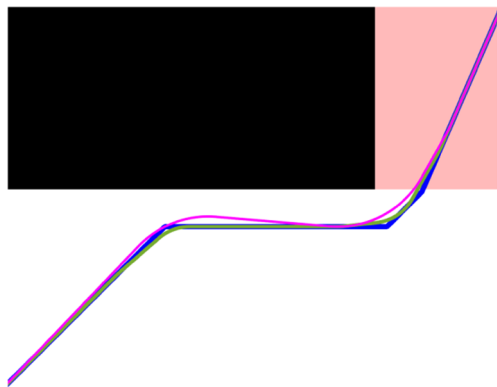


**Fig. 7** Example of the path smoothing procedure using Dubins curves. In blue the path before the smoothing procedure. In green the smoothed path with a curvature radius of 10 m, while in magenta the path with a curvature radius of 20 m

smoothing procedure can compromise the optimality of the path. On the contrary, the disadvantage is the introduction of a higher complexity in the algorithm, increasing the computation time. However, we prefer to perform the smoothing procedure after the path planning phase for two reasons: (i) the resolution of the risk-map is comparable with the curvature radius of the vehicle, so the path remains optimal; (ii) the smoothing is performed in a very short time, which is useful for the on-line adaptation of the path.

### 6 Simulation Results

This section reports simulation results, obtained through Matlab simulations and using a laptop with a 2-core with 1.9 GHz CPU.

The risk-map used in the simulations is illustrated in Fig. 8 and describes a Torino's (Italy) neighbourhood with realistic risk-costs. The risk-map has  $126 \times 76$  cells, where each element is a square cell with dimensions  $5 \times 5$  m. The risk-map is defined by coded colors: white areas are associated with minimum risk-cost, black areas have



**a**



**b**

**Fig. 8** Risk-map related to a Torino's (Italy) neighbourhood. In **a**, the urban area from Google Maps. In **b**, the realistic risk-map at 20 meters of altitude. Black pixels identify the occupied areas ( $r_c = 1$ ), while shade of red areas are associated with other risk-costs ( $0 < r_c < 1$ ), where darker red areas have a greater risk-cost

**Table 1** Results of riskA\* algorithm with different values of  $k$ 

Map	$k$	solve time [s]	path length [m]	cost	average risk-cost
Map 1 126 × 76 cells (500 simulations)	0.0	0.3010	333.7345	107.1005	0.3220
	0.5	0.2623	333.7345	107.1005	0.3220
	0.75	0.2432	333.7345	107.1005	0.3220
	1.0	0.2256	333.7525	107.1010	0.3219
	1.25	0.2066	333.7525	107.1030	0.3220
	1.5	0.1864	333.9410	107.1150	0.3218
	2.0	0.1472	334.2295	107.1945	0.3219
	2.5	0.1126	334.2990	107.5485	0.3227
Map 2 339 × 131 cells (200 simulations)	3.0	0.0814	333.7855	108.2410	0.3252
	0.0	3.3292	769.4265	220.5930	0.2864
	0.5	2.8039	769.4265	220.5930	0.2864
	0.75	2.5165	769.4265	220.5930	0.2864
	1.0	2.3007	769.5300	220.5940	0.2863
	1.25	2.1237	769.5300	220.6045	0.2864
	1.5	1.9884	769.7800	220.6225	0.2864
	2.0	1.6323	771.2785	220.7955	0.2865
	2.5	1.1328	773.3660	222.0745	0.2872
	3.0	0.6551	774.1210	223.5875	0.2888

maximum cost (obstacles and no-flight areas), while shade of red areas have middle cost, in which darker red areas are associated with higher risk costs. As reported in Section 2, the maximum acceptable probability is defined at  $10^{-6} \text{ h}^{-1}$ , consequently, zones with greater risk values are defined as no-flight areas.

Regarding the off-line path planning, the proposed riskA\* algorithm is implemented. In order to select the best value of the parameter  $k$ , a Monte Carlo simulation campaign is carried out considering a set of values of  $k$  and two maps. We execute 500 independent simulations with the map illustrated in Fig. 8b, and 200 independent simulations with the map in Fig. 11. Simulations are randomized with respect to start and goal positions. Observing numerical results in Table 1, we observe that the  $k$  parameter affects the optimized path and the time required to compute the solution. High values of  $k$  yields fast solution time at the expense of path optimality. An opposite effect is observed for low values of  $k$ . In particular, with  $k = 0$ , the heuristic function is not active and the behavior of the riskA\* is the same of the Dijkstra algorithm. With both maps, our simulations lead to select a value of  $k = 0.75$  to provide a good trade off between optimality of the solution and computation time.

According to the results reported in Table 1, the time to attain the optimal solution using riskA\* also depends on the map size, due to an increase of the size of the graph to be visited.

Further, we also compare our riskA\* algorithm with the original A\* and RA\*. The RA\* algorithm is proposed

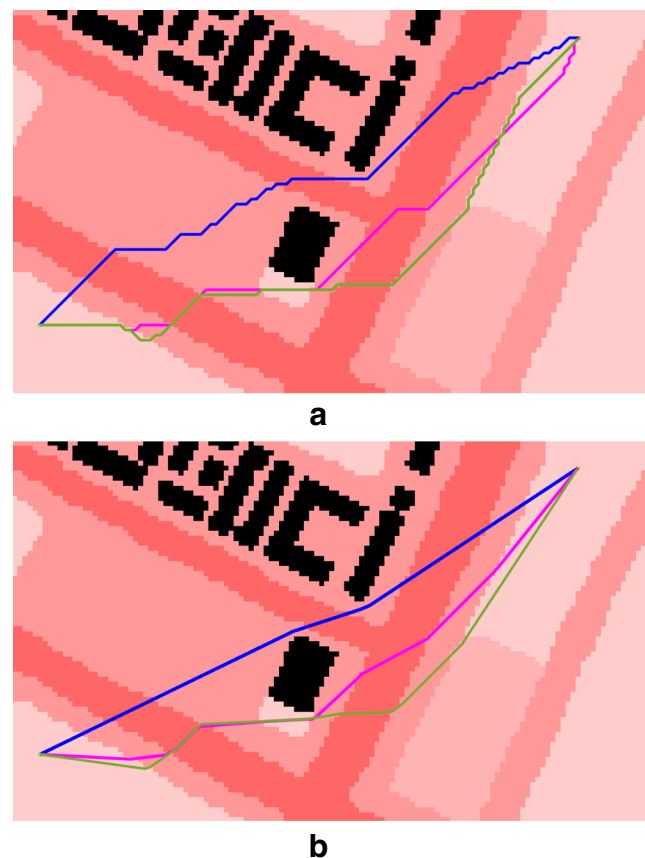


**Fig. 9** Path planning with A\* (in blue), RA\* (in magenta) and riskA\* (in green). In **a**, only the path planning algorithm is executed, while in **b** the post-optimization procedure improves the path

**Table 2** Numerical results of the simulation depicted in Fig. 9. Percentage values refer to the values of the A\* algorithm

Algorithm	solve time [s]	path length [m]	cost	average risk-cost
A*	0.5621	653.0510	254.0945	0.3883
PO A*	0.5637	608.5530 (− 6.81%)	234.6380 (− 7.65%)	0.3834 (− 1.26%)
RA*	0.4684	668.9085 (+ 2.42%)	209.9570 (− 17.37%)	0.3070 (− 20.94%)
PO RA*	0.4692	649.4940 (− 0.54%)	202.9355 (− 20.13%)	0.3098 (− 20.21%)
riskA*	0.5446	700.6245 (+ 7.2848)	196.0440 (− 22.85%)	0.2790 (− 28.14%)
PO riskA*	0.5468	674.4790 (+ 3.28%)	189.9475 (− 25.25%)	0.2781 (− 28.38%)

**Table 3** Comparison of A\*, RA\* and riskA\*. Numerical results are the average values of 500 independent simulations

Algorithm	solve time [s]	path length [m]	cost	average risk-cost
A*	0.0554	376.9025	140.5340	0.3705
PO A*	0.0755	356.6225 (− 5.38%)	133.1715 (− 5.23%)	0.3707 (+ 0.05%)
RA*	0.1964	381.8215 (+ 1.31%)	128.1155 (− 8.84%)	0.3329 (− 10.15%)
PO RA*	0.2066	367.5745 (− 2.47%)	123.2700 (− 12.28%)	0.3341 (− 9.82%)
riskA*	0.2812	392.5540 (+ 4.15%)	125.5625 (− 10.65%)	0.3220 (− 13.09%)
PO riskA*	0.2948	375.1550 (− 0.46%)	120.0565 (− 14.57%)	0.3207 (− 13.41%)

**Fig. 10** Example of the proposed risk-aware path planning approach. In **a**, riskA\* computes the off-line path (in blue). In **b**, the risk-map changes and the Borderland algorithm checks the path exploring cells around the updated area. In **c**, the path repaired by the Borderland (in blue) and the path computed from scratch with the riskA\* algorithm (in yellow) are compared. Similar behavior in **d** and **e**, whereby the risk-map is updated, and the Borderland algorithm is able to adapt the path. In **f** a detail of the path computed, where the path is smoothed with Dubins curves

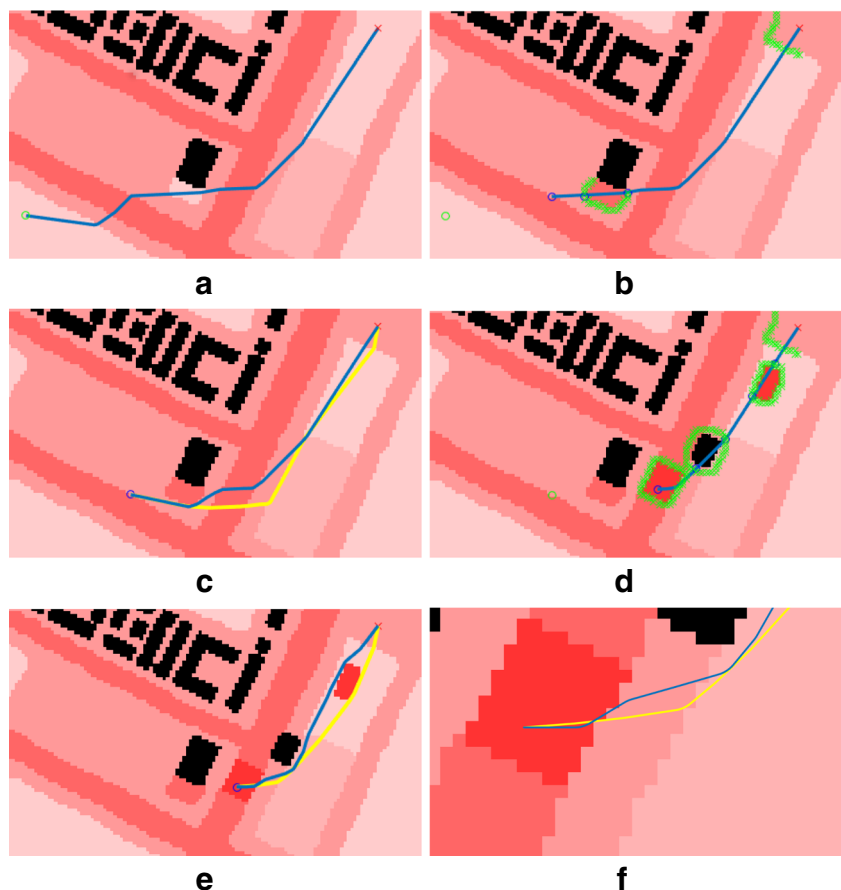


**Table 4** Results of on-line path planning

Map ID		solve time [s]	path length [m]	cost	average risk-cost
1	PO riskA*	0.8634	674.4790	189.9475	0.2781
	previous path		497.3965	165.7020	0.3336
2	PO riskA*	0.7902	530.0510	157.9735	0.2986
	Borderland	0.1932 (−75.55%)	506.5655 (−4.43%)	159.3680 (+0.88%)	0.3159 (+5.79%)
	previous path		336.5660	Invalid	Invalid
3	PO riskA*	0.2985	351.5975	98.2045	0.2839
	Borderland	0.1211 (−59.43%)	348.9715 (−0.74%)	98.4210 (+0.22%)	0.2856 (+0.60%)

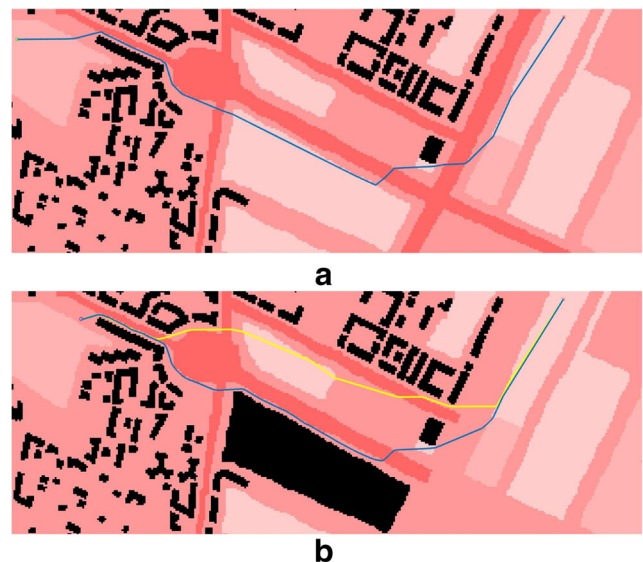
in [12] by Guglieri et al.. Similar to riskA\*, RA\* is based on original A\* and considers the risk to the population of flying over a specified area. The cost function of RA\* takes into account the risk-cost as an additive factor, whereas, in this test, the A\* algorithm optimizes the path length.

Figure 9 illustrates a comparison between the mentioned approaches. In the reported scenario, the advantage of riskA\* is apparent. According to the numerical results reported in Table 2, the riskA\* algorithm tends to compute a longer path, yet reducing the average risk-cost, as well as the motion cost.

In order to validate the proposed riskA\* algorithm, 500 independent Monte Carlo simulations are performed comparing A\*, RA\* and riskA\*, where the start and goal points are randomly sampled in the map. Test results are reported in Table 3. This test demonstrates that riskA\* is able to find the optimal path by trading off the path length and the risk-cost. Compared with the A\*-based solution, the path is longer (+4.15%), but the average risk-cost is significantly lower (−13.09%). The results show also the different behavior of the RA\* algorithm. Compared with the riskA\*, RA\* computes shorter paths, but with higher average risk-cost.

After the path planning procedure, post-optimization is performed. Figure 9b highlights the advantage of the application of the post-optimization procedure. We observe that, in the original paths in Fig. 9a, the turn angles are constrained to be expressed in multiples of 45°, while post-optimization processes the path without compromising its optimality. The advantages of the post-optimization procedure are also reported in Tables 2 and 3, performed on A\*, RA\* and riskA\*. With A\*, post-optimization only takes into account the path length, while with RA\* and riskA\* the motion cost is used, considering both path length and risk-costs. We observe that post-optimization reduces the path length and the motion cost, maintaining a comparable values of average risk-cost. Moreover, post-optimization only slightly affects the computation time of the solution.

Regarding the on-line path planning, the Borderland algorithm is implemented. Figure 10 exemplifies a scenario in which Borderland algorithm and path smoothing using Dubins curves are applied. The results displayed in the figure highlight the advantages of our approach with respect to riskA\* in executing the replanning phase. Numerical performance indicators are synthesized in Table 4, where the replanning phase is executed twice on different risk-maps. In Map 1, the path is computed using riskA\*. The risk-map is updated (Map 2) and, as a consequence, the motion cost of the path changes and the path needs to be updated. The riskA\* computes a new path from scratch, while Borderland tries to repair the older path. Referring to Table 4, the Borderland algorithm finds a solution that is not the optimal one, but the resulting motion cost is lower than the previous path. Moreover, the processing time is significantly less in respect of the riskA\* algorithm. Similar results are obtained with the third map. The path in the new map (Map 3)



**Fig. 11** Simple scenario with high dimensional map. In **a**, the path computed by riskA\*. In **b**, the path computed with Borderland (in blue) and with riskA\* (in yellow) are reported

**Table 5** Risk-aware path planning in high dimension map. Percentage values compare the Borderland with the post-optimized (PO) riskA\* algorithm

Map ID		solve time [s]	path length [m]	cost	average risk-cost
1	PO riskA*	10.7896	1813.9145	503.5395	0.2760
	previous path		1644.6530	Invalid	Invalid
2	PO riskA*	6.6231	1512.1280	447.9680	0.2966
	Borderland	0.2931 (− 95.57%)	1638.6085 (+ 8.36%)	522.9410 (+ 16.74%)	0.3174 (+ 7.01%)

is not valid and both riskA\* and Borderland update the path. RiskA\* and Borderland compute a path with similar features, but Borderland requires less computational time. In this test both post-optimization and path smoothing with Dubins curves are performed, providing a suitable path for UAVs.

The advantage of the Borderland algorithm is the fast adaptation of the path. Borderland searches for an alternative solution by exploring the local space near the involved area in the differential map. On the contrary, riskA\* computes the globally optimal path, by evaluating all the search space. For this reason, the Borderland algorithm cannot guarantee the global optimal solution. However, the advantage of Borderland is more visible with high dimension map. In Fig. 11, a simple scenario is shown using a map with  $339 \times 131$  cells. Results in Table 5 demonstrate that Borderland is faster than riskA\*. The solve time in Table 5 refers to the time required to perform the replanning, as well as both the post-optimization and path smoothing using Dubins curves. Figure 10f shows a detail of the path after the path smoothing procedure.

## 7 Conclusions and Future Works

In this paper, we have presented a risk-aware path planning strategy for UAVs in urban environments, where people and crowds are a critical safety issue. The proposed approach computes a path usable in autonomous missions and it consists of two phases, off-line and on-line path planning.

The off-line path planning searches for a globally optimal path considering the risk-map as a static environment. An A\*-based algorithm is proposed, called riskA\*. RiskA\* uses a cost function that considers both path length and risk-cost, the resulting path minimizes the combination of these two factors.

Simulation results corroborate the validity of our approach and demonstrate the good performance of riskA\*. In particular, riskA\* is able to seek for an optimal solution considering the risk to the population on the ground, a critical factor in urban environments. Results of riskA\* are also compared with RA\*, an A\*-based algorithm proposed in [12].

The on-line path planning adjusts and adapts the path considering a dynamically updated risk-map. We propose the Borderland algorithm as a solution. Toward the adaptation of the off-line trajectory to the unanticipated operational conditions, Borderland performs *check and repair* routines. First, it checks which parts of the path are involved in the dynamic risk-map, then it searches for an alternative path.

Simulation results show that Borderland is able to repair and adjust the path in a short time and in diverse scenarios, minimizing the risk-cost. Moreover, instead of computing new paths from scratch every time, Borderland adjusts the existing path only when it is necessary. This constitutes an advantage, especially in high dimensional map.

After path planning, a path smoothing procedure produces a realistic and suitable path for UAVs. Smoothing is performed using Dubins curves and modifies the path in a flyable one in short time, without compromising the optimality of the path.

The joint use of off-line and on-line path planning constitutes a valid risk-aware path planning strategy for UAVs. The resulting behavior demonstrates that the proposed approach is able to compute and maintain a valid, safe and reliable path, despite the evolution in the operational conditions.

The proposed risk-aware path planning approach solves the problem of computing and maintaining a safe path in urban environments. In particular, it guarantees to always obtain a risk level lower than the maximum acceptable risk defined, as well as to avoid no-flight zones enforced by National aviation agencies.

Future works will include the implementation of the proposed approach on a real robotic platform using the Robot Operating System (ROS) [35]. Possible improvements involve the inclusion of kinodynamic constraints of the vehicle, the presence of multiple UAVs, and the adaptation to a tridimensional environment.

**Acknowledgments** This work was supported by a fellowship from TIM, by the Siebel Energy Institute, and by Compagnia di San Paolo.

**Publisher's Note** Springer Nature remains neutral with regard to jurisdictional claims in published maps and institutional affiliations.

## References

- Buniamin, N., Wan Ngah, W., Sariff, N., Mohamad, Z.: A simple local path planning algorithm for autonomous mobile robots. *Int. J. Syst. Appl. Eng. Dev.* **5**(2), 151–159 (2011)
- Cai, G., Dias, J., Seneviratne, L.: A survey of small-scale unmanned aerial vehicles: recent advances and future development trends. *Unmanned Sys.* **2**(02), 175–199 (2014)
- Clothier, R.A., Walker, R.A., Fulton, N., Campbell, D.A.: A casualty risk analysis for Unmanned Aerial System (UAS) operations over inhabited areas. In: AIAC12, Twelfth Australian International Aerospace Congress, 2nd Australasian Unmanned Air Vehicles Conference, pp. 1–15 (2007)
- Dalamagkidis, K., Valavanis, K., Piegler, L.A.: On integrating unmanned aircraft systems into the national airspace system: issues, challenges, operational restrictions, certification, and recommendations, vol. 54. Springer Science & Business Media (2011)
- De Filippis, L., Guglieri, G., Quagliotti, F.: A minimum risk approach for path planning of UAVs. *J. Intell. Robot. Syst.* **61**(1), 203–219 (2011)
- De Filippis, L., Guglieri, G., Quagliotti, F.: Path planning strategies for UAVs in 3d environments. *J. Intell. Robot. Syst.* **65**(1), 247–264 (2012)
- Dijkstra, E.W.: A note on two problems in connexion with graphs. *Numer. Math.* **1**(1), 269–271 (1959)
- Dubins, L.E.: On curves of minimal length with a constraint on average curvature, and with prescribed initial and terminal positions and tangents. *Am. J. Math.* **79**(3), 497–516 (1957)
- Ferguson, D., Kalra, N., Stentz, A.: Replanning with RRTs. In: Proceedings 2006 IEEE International Conference on Robotics and Automation, 2006. ICRA 2006, pp. 1243–1248 (2006)
- Feyzabadi, S., Carpin, S.: Risk-aware path planning using hierarchical constrained markov decision processes. In: 2014 IEEE International Conference on Automation Science and Engineering (CASE), pp. 297–303. IEEE (2014)
- Goerzen, C., Kong, Z., Mettler, B.: A survey of motion planning algorithms from the perspective of autonomous UAV guidance. In: Selected Papers from the 2nd International Symposium on UAVs, Reno, Nevada, USA June 8–10, 2009, pp. 65–100. Springer (2009)
- Guglieri, G., Lombardi, A., Ristorto, G.: Operation oriented path planning strategies for RPAS. *Am. J. Sci. Tech.* **2**(6), 1–8 (2015)
- Guglieri, G., Ristorto, G.: Safety assessment for light remotely piloted aircraft systems. In: INAIR 2016 - International Conference on Air Transport, vol. 1, pp. 1–7 (2016)
- Hansen, K.D., la Cour-Harbo, A.: Waypoint planning with Dubins curves using genetic algorithms. In: Control Conference (ECC), 2016 European, pp. 2240–2246. IEEE (2016)
- Hart, P.E., Nilsson, N.J., Raphael, B.: A formal basis for the heuristic determination of minimum cost paths. *IEEE Trans. Syst. Sci. Cybern.* **4**(2), 100–107 (1968)
- Islam, F., Narayanan, V., Likhachev, M.: Dynamic multi-heuristic A\*. In: 2015 IEEE International Conference on Robotics and Automation (ICRA), pp. 2376–2382. IEEE (2015)
- Islam, F., Narayanan, V., Likhachev, M.: A\*-connect: bounded suboptimal bidirectional heuristic search. In: 2016 IEEE International Conference On Robotics and Automation (ICRA), pp. 2752–2758. IEEE (2016)
- Jensen, O.B.: Drone city-power, design and aerial mobility in the age of smart cities. *Geol. Helv.* **71**(2), 67 (2016)
- Karakaya, S., Ocak, H., Küçükıldız, G.: A bug-based local path planning method for static and dynamic environments. In: International Symposium on Innovative Technologies in Engineering and Science, pp 846–855. Valencia, Spain (2015)
- Karaman, S., Frazzoli, E.: Incremental sampling-based algorithms for optimal motion planning. *Robot. Sci. Syst.* **VI** **104**(2), 1–20 (2010)
- Karaman, S., Frazzoli, E.: Optimal kinodynamic motion planning using incremental sampling-based methods. In: 2010 49th IEEE Conference on Decision and Control (CDC), pp. 7681–7687. IEEE (2010)
- Kavraki, L.E., Svestka, P., Latombe, J.C., Overmars, M.H.: Probabilistic roadmaps for path planning in high-dimensional configuration spaces. *IEEE Trans. Robot. Autom.* **12**(4), 566–580 (1996)
- la Cour-Harbo, A.: Mass threshold for ‘harmless’ drones. *Int. J. Micro Air Veh.* **9**(2), 77–92 (2017)
- la Cour-Harbo, A.: Quantifying ground impact fatality rate for small unmanned aircraft. *J. Intell. Robot. Syst.* 1–18. <https://doi.org/10.1007/s10846-018-0853-1> (2018)
- LaValle, S.M.: Rapidly-exploring random trees: a new tool for path planning (1998). TR 98-11, Computer Science Dept., Iowa State University
- LaValle, S.M.: Planning algorithms. Cambridge University Press, Cambridge (2006)
- Likhachev, M., Gordon, G.J., Thrun, S.: Ara\*: anytime A\* with provable bounds on sub-optimality. In: Advances in Neural Information Processing Systems, pp. 767–774 (2004)
- Lin, Y., Saripalli, S.: Path planning using 3D Dubins curve for unmanned aerial vehicles. In: 2014 International Conference on Unmanned Aircraft Systems (ICUAS), pp. 296–304. IEEE (2014)
- Lin, Y., Saripalli, S.: Sampling-based path planning for UAV collision avoidance. *IEEE Trans. Intell. Transp. Syst.* **18**(11), 3179–3192 (2017)
- Lumelsky, V.J., Stepanov, A.A.: Path-planning strategies for a point mobile automaton moving amidst unknown obstacles of arbitrary shape. *Algorithmica* **2**(1–4), 403–430 (1987)
- Mohammed, F., Idries, A., Mohamed, N., Al-Jaroodi, J., Jawhar, I.: Uavs for smart cities: opportunities and challenges. In: 2014 International Conference on Unmanned Aircraft Systems (ICUAS), pp. 267–273. IEEE (2014)
- Murphy, R.: Introduction to AI Robotics. MIT Press, Cambridge (2000)
- Pereira, A.A., Binney, J., Hollinger, G.A., Sukhatme, G.S.: Risk-aware path planning for autonomous underwater vehicles using predictive ocean models. *J. Field Rob.* **30**(5), 741–762 (2013)
- Primates, S., Capello, E., Antonini, R., Gaspardone, M., Guglieri, G., Rizzo, A.: A cloud-based framework for risk-aware intelligent navigation in urban environments. In: 2017 International Conference on Unmanned Aircraft Systems (ICUAS), pp. 447–455. IEEE (2017)
- Quigley, M., Conley, K., Gerkey, B., Faust, J., Foote, T., Leibs, J., Wheeler, R., Ng, A.Y.: Ros: an open-source robot operating system. In: ICRA Workshop on Open Source Software, vol. 3, p. 5 (2009)
- Rathbun, D., Kragelund, S., Pongpunwattana, A., Capozzi, B.: An evolution based path planning algorithm for autonomous motion of a UAV through uncertain environments. In: The 21st Digital Avionics Systems Conference, 2002. Proceedings, vol. 2, pp. 8D2–8D2. IEEE (2002)
- Rudnick-Cohen, E., Herrmann, J.W., Azarm, S.: Risk-based path planning optimization methods for unmanned aerial vehicles over inhabited areas. *J. Comput. Inf. Sci. Eng.* **16**(2), 21004–21010 (2016)
- Savkin, A.V., Huang, H.: The problem of minimum risk path planning for flying robots in dangerous environments. In: 2016 35th Chinese Control Conference (CCC), pp. 5404–5408. IEEE (2016)
- Silva Arantes, J.D., Silva Arantes, M.D., Motta Toledo, C.F., Júnior, O.T., Williams, B.C.: Heuristic and genetic algorithm approaches for UAV path planning under critical situation. *Int. J. Artif. Intell. Tools* **26**(01), 1760008 (2017)

40. Stentz, A.: Optimal and efficient path planning for unknown and dynamic environments. Tech. rep., DTIC Document (1993)
41. Sujit, P., Saripalli, S., Sousa, J.B.: Unmanned aerial vehicle path following: a survey and analysis of algorithms for fixed-wing unmanned aerial vehicles. *IEEE Control. Syst.* **34**(1), 42–59 (2014)
42. Weiß, B., Naderhirn, M., del Re, L.: Global real-time path planning for UAVs in uncertain environment. In: *Computer Aided Control System Design, 2006 IEEE International Symposium on Control Applications, 2006 IEEE International Symposium on Intelligent Control, 2006 IEEE*, pp. 2725–2730. IEEE (2006)
43. Wen, N., Su, X., Ma, P., Zhao, L., Zhang, Y.: Online UAV path planning in uncertain and hostile environments. *Int. J. Mach. Learn. Cybern.* **8**(2), 469–487 (2017)
44. Wzorek, M., Doherty, P.: Reconfigurable path planning for an autonomous unmanned aerial vehicle. In: *International Conference on Hybrid Information Technology, 2006. ICHIT'06*, vol. 2, pp. 242–249. IEEE (2006)
45. Yang, L., Qi, J., Xiao, J., Yong, X.: A literature review of UAV 3D path planning. In: *2014 11th World Congress on Intelligent Control and Automation (WCICA)*, pp. 2376–2381. IEEE (2014)
46. Zhang, B., Mao, Z., Liu, W., Liu, J.: Geometric reinforcement learning for path planning of UAVs. *J. Intell. Robot. Syst.* **77**(2), 391–409 (2015)

**Stefano Primatesta** is currently a Ph.D. student in Computer and Control Engineering at the Politecnico di Torino, Italy. He received his B.S in Electronic Engineering and the M.S. in Mechatronic Engineering from Politecnico di Torino in 2011 and 2014, respectively. His research interests include autonomous navigation and service robotics, with applications on unmanned aerial vehicles and unmanned ground vehicles.

**Giorgio Guglieri** is currently a Full Professor of Politecnico di Torino, Italy, in the Department of Mechanical and Aerospace Engineering. He received his M.S. degrees from Politecnico di Torino in 1989. His research interests include flight mechanics, unmanned aerial vehicles and space systems. He is a Senior Member of AIAA and a Member of AHS.

**Alessandro Rizzo** is an Associate Professor in the Department of Electronics and Telecommunications at Politecnico di Torino, Italy. He received the “Laurea” degree (summa cum laude) in computer engineering and the Ph.D. degree in automation and electronic engineering from the University of Catania, Italy, in 1996, and 2000, respectively. In 1998, he worked as EURATOM Research Fellow at JET Joint Undertaking, Abingdon, U.K., researching on sensor validation and fault diagnosis for nuclear fusion experiments. In 2000 and 2001, he worked as Research Consultant to ST Microelectronics, Catania Site, Italy, and as Industry Professor of Robotics at the University of Messina, Italy. From 2002 to 2015 he was a tenured Assistant Professor at Politecnico di Bari, Italy. In November 2015, he joined Politecnico di Torino. From 2012, he has also been a Visiting Professor at New York University Tandon School of Engineering, Brooklyn NY, USA. Prof. Rizzo is engaged in conducting and supervising research on complex networks and systems, modeling and control of nonlinear systems, cooperative robotics. He is author of two books, two international patents, and more than 130 papers on international journals and conference proceedings. Prof. Rizzo has been the recipient of the award for the best application paper at the IFAC world triennial conference in 2002 and of the award for the most read papers in Mathematics and Computers in Simulation (Elsevier) in 2009. Prof. Rizzo is also a Distinguished Lecturer of the IEEE Nuclear and Plasma Science Society.